Interpreting the Conductance Blockades of DNA Translocations Through Solid-State Nanopores

By: Autumn T. Carlsen, Osama K. Zahid, Jan Ruzicka, Ethan W. Taylor, and Adam R. Hall

Autumn T. Carlsen, Osama K. Zahid, Jan Ruzicka, Ethan W. Taylor, and Adam R. Hall. Interpreting the Conductance Blockades of DNA Translocations Through Solid-State Nanopores. *ACS Nano* 2014, 8, 5, 4754–4760. https://doi.org/10.1021/nn501694n

Abstract:

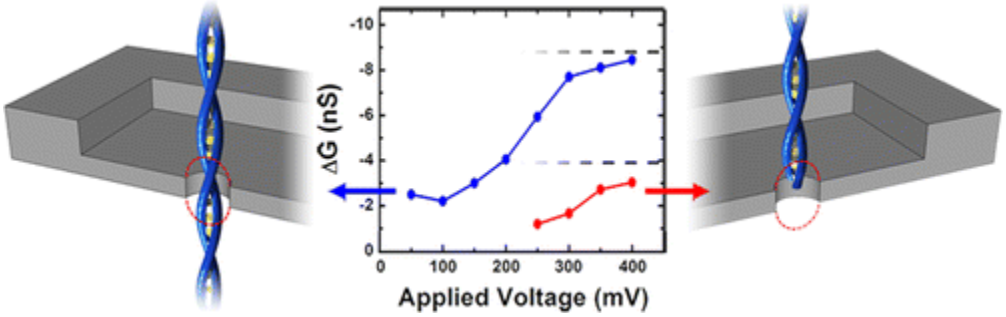

Solid-state nanopore electrical signatures can be convoluted and are thus challenging to interpret. In order to better understand the origin of these conductance changes, we investigate the translocation of DNA through small, thin pores over a range of voltage. We observe multiple, discrete populations of conductance blockades that vary with applied voltage. To describe our observations, we develop a simple model that is applicable to solid-state nanopores generally. These results represent an important step toward understanding the dynamics of the electrokinetic translocation process.

Keywords: nanopore | DNA | translocation | conductance blockade | single molecule

Article:

Solid-state nanopores[1, 2] are an emerging technology for rapid detection and characterization of biomolecules. In a typical measurement, an electric field is employed to drive individual molecules of RNA,[3] proteins,[4-7] and most often DNA[8, 9] through a single aperture in a solid-state membrane (Figure 1a). The brief presence of the molecule within the opening is manifested as a shift in the measured electrical signal to one or more distinct levels of conductance, referred

to as a blockade event. By virtue of their size, SS-nanopores are able to interrogate one or a few individual molecules at a time, and so they have proven to be an attractive possibility for a range of applications that require highly sensitive detection, perhaps most notably genetic sequencing.[10]

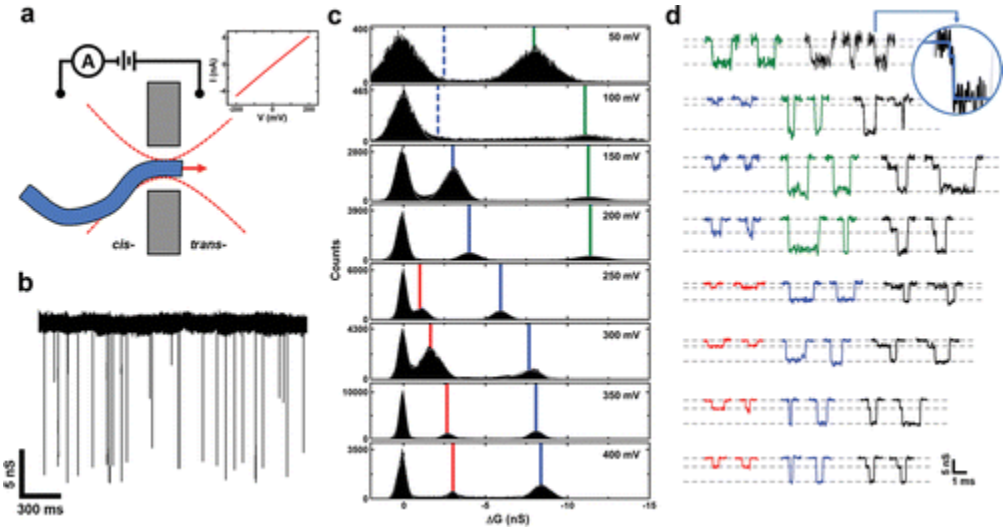

Figure 1. Conductance blockade measurements of dsDNA (a) Schematic representation of electrokinetic translocation from the *cis*- side of a SS-nanopore membrane to the *trans*- side. Inset shows the linear I–V characteristics of the device used here. (b) Typical conductance trace measured for 3 kbp dsDNA using a 4.5 nm thick, 3.4 nm diameter SS-nanopore. Voltage is 400 mV. (c) All-points histograms of (concatenated) conductance blockades from 50 to 400 mV (low-pass filtered at 10 kHz). In each panel, the left-most peak corresponds to the baseline (open-pore) conductance. Vertical lines indicate the center of the Gaussian fit (gray line) and indicate the evolution of individual conductance populations designated by color. (d) Example event traces for each applied voltage in (c). Dashed lines in background designate the discrete populations from the histograms to the left. Trace colors indicate the conductance level population of the event from (c), except the black traces, which correspond to events containing more than one level. The inset offers a magnified view of the indicated combination event, highlighting the brief initial shallow level. Note that this level is not resolvable in the 50 or 100 mV histograms (see text), but its position is indicated by dashed blue lines. All traces are low-pass filtered at 20 kHz. The scale bar applies to all traces.

Although the operating principle of SS-nanopores is straightforward, the system is capable of exhibiting surprisingly complex behaviors that can make interpretation of the measured electrical signal challenging. One source of this complexity is thought to be interactions with the access regions[11]—the sensing volume immediately surrounding each opening of the aperture. Here, we seek to shed light on SS-nanopore measurements in general by investigating double-strand (ds) DNA conductance blockades systematically using a nanopore device with maximized contributions of the access regions to the sensing region. The access regions have long been an important consideration[12] in describing both cylindrical[13-19] and noncylindrical[20-23] nanopore systems. However, for SS-nanopores in extremely thin membranes[19] (<10 nm), these regions take on increased significance. We therefore initiate our study of conductance depth (ΔG) by investigating these unconventional devices.

Results and Discussion

We begin by measuring 3 kbp dsDNA under high-ionic strength conditions with a single SS-nanopore (diameter 3.4 nm) fabricated in a 4.5 nm thick membrane. Previous work on devices with similar dimensions and under comparable solvent conditions demonstrated that dsDNA translocations produce deeper blockade events[19, 24] compared to the typical 1–2 nS depth measured in conventional (thick) membranes.[3, 8, 9] Our measurements confirm this observation in general (Figure 1b). However, we arrive at a substantially more complex picture when we investigate the dependence of ΔG on applied voltage. Figure 1c shows all-points histograms for (concatenated) events over the range of 50–400 mV, with Gaussian fits (gray lines) indicating the locations of discrete conductance levels. From these data, we make two observations. First, we generally do not observe that the conductance blockade level resides exclusively at a single level, as may be expected for head-to-tail translocation of dsDNA through an aperture that is too narrow to allow the passage of folded molecules. Instead, we observe two well-separated levels of conductance under most conditions. These levels are not mutually exclusive, however, as we note that combination events occur regularly (black traces in Figure 1d). Second, the ΔG levels themselves shift significantly as the applied voltage is increased. Examining the evolution of blockade levels as a function of voltage (Figure 1c) reveals that three distinct populations are detected, each of which appears to increase in depth as applied voltage is increased.

We address the first of these observations by hypothesizing that the plurality of conductance blockade levels is the result of nontranslocative interactions with our device. This hypothesis is supported by the observed voltage dependence of mean event dwell time measurements (see the Supporting Information, Figure S-2). Recent work from several groups has suggested that unexpected levels of ΔG measured under certain experimental conditions are a result of dsDNA entering the access region, either stochastically[25, 26] or as a precursor to translocation.[27-29] In order to describe the conductance blockades that may be expected from this type of interaction, we utilize a model in which the SS-nanopore sensing region is composed of three relevant sections, the interior of the nanopore itself and the two access regions on either side (Figure 2a), following past work.[14, 17] The conductance of each access region can be expressed simply[11] as

$$G_{0_{\mathrm{acc}}} = 2\sigma d_{\mathrm{p}} \tag{1}$$

where d_{p} is nanopore diameter and σ is the conductivity of the solution, defined as $(\mu_{\mathrm{cation}} + \mu_{\mathrm{anion}})ne$. Here, n is the number density (proportional to concentration) of the ionic species, e is the elementary charge, and μ_{cation} and μ_{anion} are electrophoretic mobilities of the cation and anion, respectively. The conductance of the pore, meanwhile, is

$$G_{0_{\mathrm{pore}}} = \frac{\pi d_{\mathrm{p}}^2}{4L_{\mathrm{eff}}}\left(\sigma + \frac{4S\mu_{\mathrm{cation}}}{d_{\mathrm{p}}}\right) \tag{2}$$

where L_{eff} is the effective thickness of the membrane and S is the surface charge density[30] of the nanopore walls (taken[31] as 0.06 C/m^2). We use the convention of Wanunu *et al.*[19] who established experimentally that $L_{\mathrm{eff}} = L/3$, where L is the initial membrane thickness, to account

for the noncylindrical shape of the nanopore. Because these conductances are in series, the total open-pore conductance of the system can thus be written as

$$G_{0_{\mathrm{TOTAL}}} = \left(\frac{1}{G_{0_{\mathrm{pore}}}} + \frac{2}{G_{0_{\mathrm{acc}}}} \right)^{-1} \tag{3}$$

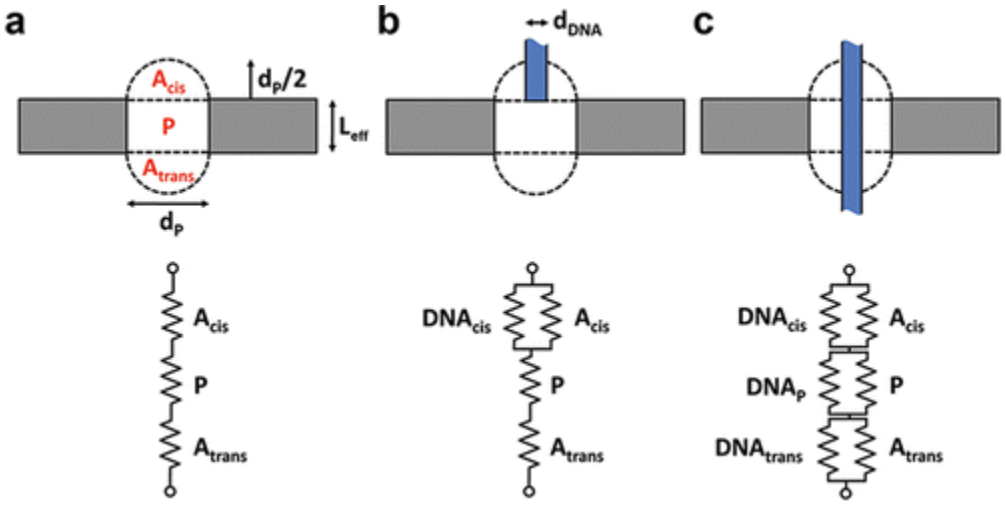

Figure 2. Components of the model. (a) Schematic of the three series conductances that form the sensing region of a SS-nanopore (gray): the pore (*P*) and the two hemispherical access regions (A_{cis} and A_{trans}, respectively). Models of DNA interaction with (b) one access region only (*case 1* from the text) and (c) all three regions (*case 2* from the text). Below each diagram is an equivalent circuit (conductances shown as resistors) representing the contributions of the three sensing regions listed above as well as that of the presence of the DNA in A_{cis} (designated DNA_{cis}), *P* (designated DNA_{P}), and A_{trans} (designated DNA_{trans}). Not shown are contributions of counterions surrounding the DNA, which act as an additional parallel conductance in each of the three regions.

Generally, the presence of dsDNA in any of the sensing regions described above will act as a negative parallel conductance, displacing volume that would otherwise contribute to the total measured conductance. In order to quantify the effect, we consider two basic scenarios in relation to our data, taking into account that conductance can be expressed generally as $\sigma(A/l)$, where A is area and l is length.

In *case 1* (Figure 2b), the dsDNA is positioned coaxially with the mouth of the pore such that it interacts only with a single access region. Although the dsDNA could adopt a range of orientations with respect to this region, the geometry considered here can be considered a maximimum as it occupies the most space within the access region. In this scenario, the effect on the conductance of the occluded access region is

$$G_{\mathrm{acc}_{\mathrm{DNA}}} = G_{0_{\mathrm{acc}}} - G_{\mathrm{DNA}_{\mathrm{acc}}} = G_{0_{\mathrm{acc}}} - \sigma \frac{\pi d_{\mathrm{DNA}}^2}{2 d_{\mathrm{p}}} \tag{4}$$

where d_{DNA} is the diameter of dsDNA, taken to be 2.2 nm. Note that in this case, the pertinent length of DNA, l, is the length of the access region ($d_p/2$). All other regions will be unchanged. As a result, the total change in conductance can be expressed as

$$\Delta G_{case1} = \left(\frac{1}{G_{0_{\text{pore}}}} + \frac{1}{G_{0_{\text{acc}}}} + \frac{1}{G_{\text{acc}_{\text{DNA}}}} \right)^{-1} - G_{0_{\text{TOTAL}}} \tag{5}$$

In *case 2*, the dsDNA is present in all three regions of the system (Figure 2c). As such, both access regions are affected as described in eq 4, and additionally, the conductance of the nanopore region is altered, as described by

$$G_{\text{pore}_{\text{DNA}}} = G_{0_{\text{pore}}} - G_{\text{DNA}_{\text{pore}}} = G_{0_{\text{pore}}} - \sigma \frac{\pi d_{\text{DNA}}^2}{4L_{\text{eff}}} \tag{6}$$

In total, this results in an expected conductance change for *case 2* of

$$\Delta G_{case2} = \left(\frac{1}{G_{\text{pore}_{\text{DNA}}}} + \frac{2}{G_{\text{acc}_{\text{DNA}}}} \right)^{-1} - G_{0_{\text{TOTAL}}} \tag{7}$$

The intermediate case, in which the dsDNA resides only in the *cis*-side access region and the nanopore is transitional since passage to the *trans*-side access region (*i.e., case 2*) is almost immediate from this state. As such, we consider it unlikely to be observed.

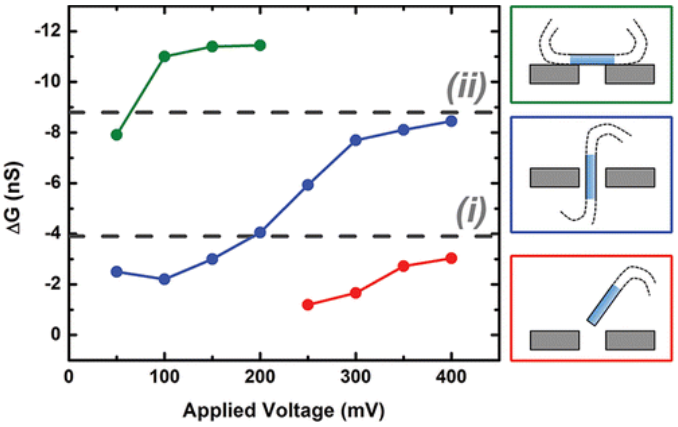

Figure 3. Analysis of dsDNA conductance blockades (a) Mean conductance change *vs* applied voltage. The dashed lines (*i*) and (*ii*) represent the calculated ΔG from eqs 5 (*case 1*, corresponding to nontranslocative events) and 7 (*case 2*, corresponding to translocation), respectively. Each point is the center of a Gaussian fit to the relevant histogram of all recorded events in Figure 1c, except the blue points at 50 and 100 mV, which are Gaussian fit centers from an all-points histogram of events containing the lower (2–2.5 nS) level. Schematics to the right illustrate the DNA configuration we propose for each population. Colors match those in in Figure 1c.

Equations 5 and 7 can be applied to our data by incorporating the device dimensions (d_p = 3.4 nm, $L_{eff} = L/3$ = 1.5 nm) and solvent conditions used in the experiment. Doing so yields for *case 1* a ΔG of −3.9 nS and for *case 2* a ΔG of −8.8 nS. In Figure 3a, we plot the mean conductance blockade levels over all investigated voltages, showing that the measured ΔG of each population increases and then saturates. Strikingly, the conductance levels predicted by our simple model (dashed lines in Figure 3a) match very closely the saturation conductance observed for two of the event populations from the experimental data. This indicates that at high voltages (≥250 mV) for our device, the large ΔG level corresponds to true molecular translocations while the low ΔG level indicates nontranslocative interactions with the access region. We note that this model can be used similarly to predict the apparent saturation conductance change for results on voltage dependence of ΔG published elsewhere[3, 32, 33] (see the Supporting Information, Figure S-3).

Our model accounts for two populations within our data, but what is the origin of the third? One possibility may be that this level of conductance blockade is caused by a molecule approaching the SS-nanopore such that it lays perpendicular to the axis of the aperture.[25, 27-29, 34] In this case, the stiffness of the molecule would prevent it from passing through the pore in a folded state, but the ion conductance would be blocked by its presence. The simplest approximation of this arrangement is that the area occupied by the dsDNA above the opening reduces the effective diameter of the SS-nanopore during its residence. If we assume a circular pore in the blocked case, this reduced effective pore diameter, d^*_p, can be expressed geometrically (see the Supporting Information, Figure S-4) by the equation

$$d_p^* = \sqrt{\frac{2}{\pi}\left(d_p^2 \cos^{-1}\left(\frac{d_{DNA}}{d_p}\right) - d_{DNA}\left(d_p^2 - d_{DNA}^2\right)^{1/2}\right)} \tag{8}$$

This assumes that the dsDNA sits directly across the center of the SS-nanopore. We arrive at an expected ΔG for the perpendicular case by simply calculating the difference between the conductance of the unoccluded pore with diameter d_p and the conductance of a pore with diameter d^*_p using eq 3. For our experimental conditions, ΔG for lateral blocking of the pore is found to be −15 nS. Since this can be considered a maximum (*i.e.*, the dsDNA may not interact symmetrically across the center of the pore), the value is in qualitative agreement with the maximum conductance blockade recorded for the uncategorized population in Figure 3a of about −12 nS. We therefore conclude that this population is likely to correspond to lateral, nontranslocative interactions of the dsDNA with the SS-nanopore.

Identification of each conductance population presents further insight into the translocation process. As seen in Figure 1d, discrete conductance levels occur not only independently in single-level events, but also in combination to form two-level events. Interestingly, we observe that the shallow conductance level precedes the deep level for nearly all two-level events recorded across the entire investigated voltage range (543 out of 553, or 98.2%). At high voltages (≥250 mV), this ordering suggests an initial time period during which the end of the dsDNA is positioned in the access region of the SS-nanopore prior to threading through the aperture. The initial lag may correspond to repositioning or unfolding of the ensuing length of the molecule[35, 36] (see the Supporting Information, Figure S-5). At low voltages (≤200 mV), the shallow-to-deep progression of conductance levels suggests instead that a portion of the dsDNA

is threaded through the nanopore prior to lateral interactions between the remainder of the molecule and the aperture. We attribute these lateral interactions to the diminished capacity of the low-voltage electric field gradient to overcome the entropy of the dsDNA near the SS-nanopore.[26] Thus, the end of a threading molecule drags the entropic coil to the aperture *en bloc*, where it creates a deeper blockade as the translocation process continues. As voltage is reduced further, the likelihood of a molecular end being made available by the weaker electric field gradient is also reduced. Thus, at very low voltage, we would expect the shallow event level corresponding to translocation to be rare. This is indeed the case; the translocation ΔG level is uncommon at both 50 and 100 mV, and in conjunction with the low signal-to-noise ratio at these voltages, it is not distinguishable in an all-points histogram (see Figure 1c). However, the lower level can be resolved within individual blockade events (Figure 1d, top panel). Besides serving as additional support for our interpretation, this observation also offers an explanation as to why the ΔG level corresponding to lateral interactions with the SS-nanopore is seen exclusively at low voltage: at voltages greater than 200 mV, the large electric field gradient and increased viscous drag act to uncoil the dsDNA in solution before it reaches the pore.[37] Note that the deep ΔG level does not necessarily preclude molecular translocation at low voltage. Indeed, the blockade caused by the entropic coil may be able to simply mask the signal of the simultaneous threading of dsDNA through the pore.

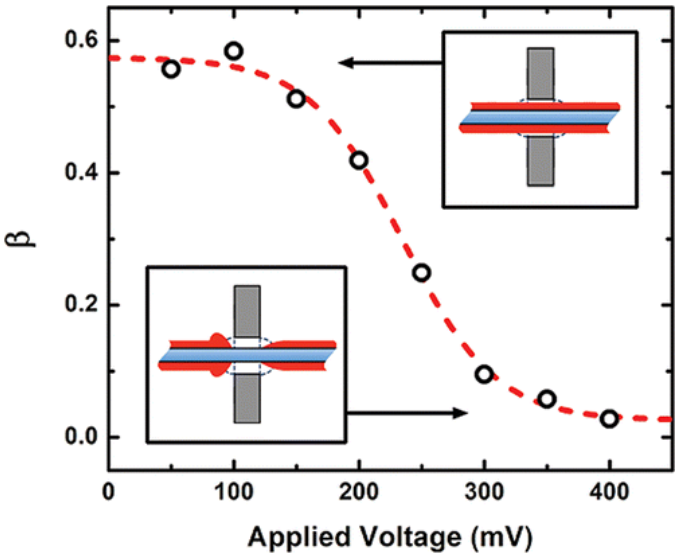

Figure 4. Counterion residence on translocating dsDNA The fraction of Na counterion charge (relative to the charge density of the dsDNA backbone) β *vs* applied voltage. Dashed line is a Boltzmann sigmoid fit to the data. Insets show schematic interpretation of the low-voltage case (top), where counterions remain bound to the DNA, and the high-voltage case (bottom), where counterions are displaced locally during translocation. In both images, DNA motion is toward the right. A more detailed schematic treatment is provided in the Supporting Information (Figure S-6).

While our model explains a great deal of what we observe in experiment, one central question remains: why do the conductance blockade levels increase and then saturate with applied voltage? Recently, several groups have reported similar behavior in conventional SS-nanopores,[3, 32, 33] but so far, an explanation has not been agreed upon. We suggest that the origin of this effect may be polarization of the dsDNA counterion cloud. The presence of positive

charges surrounding the negatively charged dsDNA backbone is known to counteract the conductance blockade by introducing additional carriers to the sensing region.[30] However, theoretical work by Mendel[38] and later refinement by Manning[39] and others[40, 41] has predicted that the local density of these counterions can be perturbed under extreme electric fields. Counterion polarization has since been observed through simulation[42-44] and experiment[45-47] and has recently been suggested as a potential factor in SS-nanopore measurements as well.[48, 49] Perturbation of the counterion cloud could remove charge carriers locally from the sensing region of a nanopore, resulting in a voltage-dependent conductance blockade. Note that this local perturbation does not contradict overall electroneutrality as has been observed in molecular dynamics simulations.[50, 51] Rather, the reduction in counterion density local to the sensing region of the nanopore would be accompanied by an equivalent buildup of charge outside the sensing region, as shown schematically in Figure 4 and in more detail in Figure S-6 (Supporting Information). In addition, because polarization will saturate at very high electric field strength,[39] the voltage-dependence would likewise saturate at high voltage. These two key expectations match our experimental results well.

Counterion screening and polarization can be included in our model through a simple adjustment to eqs 4 and 6

$$G_{\mathrm{acc_{DNA}}} = G_{0_{\mathrm{acc}}} - G_{\mathrm{DNA_{acc}}} + G_{\mathrm{counter_{acc}}} = G_{0_{\mathrm{acc}}} - G_{\mathrm{DNA_{acc}}} + \beta \frac{2q\mu_{\mathrm{cation}}}{d_{\mathrm{p}}} \tag{9}$$

$$G_{\mathrm{pore_{DNA}}} = G_{0_{\mathrm{pore}}} - G_{\mathrm{DNA_{pre}}} + G_{\mathrm{counter_{pore}}} = G_{0_{\mathrm{pore}}} - G_{\mathrm{DNA_{pore}}} + \beta \frac{q\mu_{\mathrm{cation}}}{L_{\mathrm{eff}}} \tag{10}$$

where q is the charge per unit length of dsDNA. We introduce β to denote the fractional effect of the new term relative to the zero-field counterion density, indicating polarization-induced depletion in the sensing region of the nanopore. When β = 1, the charge of the counterion cloud is exactly equivalent to that of the dsDNA itself. When β = 0, no counterions are present on the dsDNA in the sensing region and volumetric blocking is the only contribution to the conductance change (an alternative conceptualization is that β is indicative of a voltage-dependent shift in counterion mobility μ_{cation} rather than total counterion residence in the sensing region, though it is unclear by what mechanism this effect might saturate). So far, our model has assumed intrinsically that β = 0, resulting in good agreement with measurements at high voltage where polarization fully depletes of counterions in the pore. The transition toward this state can be analyzed further by using eqs 9 and 10 to determine the β necessary to account for the measured voltage dependence of the ΔG. Such an analysis (Figure 4) suggests that the fractional residence of counterions around the dsDNA in the sensing region of the SS-nanopore decreases with voltage in a sigmoidal fashion. This data can be extrapolated to yield the zero-field value, which is β = 0.57 for our system. This value may be indicative of the fraction of counterions relative to the total dsDNA charge in the sensing region that are bound tightly to the molecule (resident in the major and minor grooves,[52] for example) under our solvent conditions (see the Supporting Information, Figure S-7). We note that β would represent an axial average along the length of the sensing region due to the axial inhomogeneity of the electric field in the nanopore. This approach may offer a general route toward probing the screening of polymers and biopolymers by arbitrary ionic species at various concentrations.

Conclusions

In conclusion, we have investigated dsDNA conductance blockades with a small diameter (3.4 nm) SS-nanopore formed in a thin (4.5 nm) membrane. We measured across a range of applied voltage and found that (i) three discrete levels of conductance change can be observed and (ii) the ΔG associated with these levels becomes larger as the voltage is increased. We presented a simple model that takes into account the access regions of the SS-nanopore device and considers both the volume of the dsDNA and its accompanying countercharge layer as parallel conductances to that of the nanopore itself. We found that this model describes accurately the conductance blockade levels measured experimentally and additionally provides a possible explanation for the observed voltage dependence of ΔG. We proposed that the intensifying electric field that accompanies increasing voltage progressively removes the counterions surrounding the dsDNA in solution until eventually ion exclusion is the only contribution to the measured conductance change. Our results are widely applicable to a variety of experimental conditions and represent an important step toward understanding the meaning of SS-nanopore electrical signals in general. Indeed, our model can also be used to describe the observations of several previous studies using a variety of experimental conditions (see the Supporting Information, Figures S-3 and S-8). We note that while qualitative agreement is observed in all ionic conditions, quantitative agreement between our model and experimental work is currently limited to high-ionic strength solutions (see the Supporting Information, Figure S-9). Extension to the low-ionic strength regime should be possible with refinement.

In conventional systems, the multiple conductance blockade populations described here will be subtle. For example, under typical solvent conditions (1 M KCl) for a SS-nanopore device with diameter and membrane thickness values of 20 nm each, the ΔG predicted for nontranslocative interactions with the access region would be expected to have a maximum value of only −0.7 nS in the high-voltage ($\beta = 0$) limit. Event duration would also be expected to be very brief under these high voltage conditions, and so as a result, reduction of the noise floor to a point where such events would be measurable is likely to filter them out entirely. This may explain why the effect has not been described previously. As device diameter or membrane thickness is reduced, however, the influence of the access regions will become more conspicuous. For this reason, the current trend of the field toward SS-nanopore devices with small diameters[53] or low dimensionality[54-58] will be especially aided by consideration of our findings in order to assess results accurately.

Materials and Methods

Solid-State Nanopore Fabrication

Silicon chips, each supporting a window of silicon nitride (24.5 nm thick as measured by ellipsometry), were purchased commercially (Norcada, Inc., Alberta, Canada). Thin SS-nanopores were produced with helium ion microscope fabrication by first reducing the local membrane thickness controllably[59] and then milling material from the center of the thinned region using a timed exposure.[33] The region around the pore was processed to have a final thickness of 4.5 ± 0.6 nm, as judged by two separate calibration strategies.[59, 60] The precise

diameter of the SS-nanopore was determined by applying the measured current–voltage characteristics of the device to eq 3 from the text and solving for d_p. The device exhibited a linear I–V curve and had a low-noise baseline conductance of 27.5 nS that varied less than 5% during the duration of the measurements.

DNA Translocation Measurements

Solvent conditions used for the presented measurements were 900 mM NaCl, 10 mM tris, 1 mM EDTA. dsDNA (3 kbp) was introduced to the *cis* side of the SS-nanopore at a concentration of ~10 ng/μL. Conductance blockade events were recorded at a bandwidth of 200 kHz and with a 100 kHz four-pole Bessel filter applied. An additional low-pass filter of 10–20 kHz was applied during analysis (as indicated in figure captions), which was performed using custom LabView software. Histograms from Figure 1c (and scatter plots in the Supporting Information, Figure S-1) are composed of n = 96 (50 mV), 146 (100 mV), 426 (150 mV), 298 (200 mV), 437 (250 mV), 814 (300 mV), 542 (350 mV), and 616 (400 mV). Only events with durations between 100 μs and 2 ms were considered in our analysis.

Acknowledgment

A.R.H. acknowledges startup funds from the Wake Forest University School of Medicine. E.W.T. and J.R. acknowledge funding from The Dr. Arthur and Bonnie Ennis Foundation, Decatur, IL. We thank U. F. Keyser for critical reading of the manuscript and M. Wanunu for supplying data for analysis in Figure S-5 (Supporting Information).

References

1. Dekker, C. Solid-State Nanopores Nat. Nanotechnol. **2007**, 2, 209– 215 Google Scholar
2. Wanunu, M. Nanopores: A Journey Towards DNA Sequencing Phys. Life Rev. **2012**, 9, 125– 158 Google Scholar
3. Skinner, G. M.; van den Hout, M.; Broekmans, O.; Dekker, C.; Dekker, N. H. Distinguishing Single- and Double-Stranded Nucleic Acid Molecules Using Solid-State Nanopores Nano Lett. **2009**, 9, 2953– 2960 Google Scholar
4. Firnkes, M.; Pedone, D.; Knezevic, J.; Doeblinger, M.; Rant, U. Electrically Facilitated Translocations of Proteins Through Silicon Nitride Nanopores: Conjoint and Competitive Action of Diffusion, Electrophoresis, and Electroosmosis Nano Lett. **2010**, 10, 2162– 2167 Google Scholar
5. Fologea, D.; Ledden, B.; McNabb, D. S.; Li, J. Electrical Characterization of Protein Molecules By a Solid-State Nanopore Appl. Phys. Lett. **2007**, 91 Google Scholar
6. Han, A. P.; Schurmann, G.; Mondin, G.; Bitterli, R. A.; Hegelbach, N. G.; de Rooij, N. F.; Staufer, U. Sensing Protein Molecules Using Nanofabricated Pores Appl. Phys. Lett. **2006**, 88 Google Scholar

7. Plesa, C.; Kowalczyk, S. W.; Zinsmeester, R.; Grosberg, A. Y.; Rabin, Y.; Dekker, C. Fast Translocation of Proteins Through Solid-State Nanopores Nano Lett. **2013**, 13, 658– 663 Google Scholar

8. Li, J. L.; Gershow, M.; Stein, D.; Brandin, E.; Golovchenko, J. A. DNA Molecules and Configurations in a Solid-State Nanopore Microscope Nat. Mater. **2003**, 2, 611– 615 Google Scholar

9. Storm, A. J.; Chen, J. H.; Zandbergen, H. W.; Dekker, C. Translocation of Double-Strand DNA through a Silicon Oxide Nanopore Phys. Rev. E **2005**, 71 Google Scholar

10. Branton, D.; Deamer, D. W.; Marziali, A.; Bayley, H.; Benner, S. A.; Butler, T.; Di Ventra, M.; Garaj, S.; Hibbs, A.; Huang, X.The Potential and Challenges of Nanopore Sequencing Nat. Biotechnol. **2008**, 26, 1146– 1153 Google Scholar

11. Hall, J. E. Access Resistance of a Small Circular Pore J. Gen. Physiol. **1975**, 66, 531– 532 Google Scholar

12. Willmott, G. R.; Smith, B. G. Comment on 'Modeling the Conductance and DNA Blockade of Solid-State Nanopores' Nanotechnology **2012**, 23, 088001 Google Scholar

13. Bacri, L.; Oukhaled, A. G.; Schiedt, B.; Patriarche, G.; Bourhis, E.; Gierak, J.; Pelta, J.; Auvray, L. Dynamics of Colloids in Single Solid-State Nanopores J. Phys. Chem. B **2011**, 115, 2890– 2898 Google Scholar

14. Hyun, C.; Rollings, R.; Li, J. Probing Access Resistance of Solid-State Nanopores With a Scanning-Probe Microscope Tip Small **2012**, 8, 385– 392 Google Scholar

15. Kowalczyk, S. W.; Grosberg, A. Y.; Rabin, Y.; Dekker, C. Modeling the Conductance and DNA Blockade of Solid-State Nanopores Nanotechnology **2011**, 22, 315101 Google Scholar

16. Sun, L.; Crooks, R. M. Single Carbon Nanotube Membranes: A Well-Defined Model for Studying Mass Transport Through Nanoporous Materials J. Am. Chem. Soc. **2000**, 122, 12340– 12345 Google Scholar

17. Tsutsui, M.; Hongo, S.; He, Y.; Taniguchi, M.; Gemma, N.; Kawai, T. Single-Nanoparticle Detection Using a Low-Aspect-Ratio Pore ACS Nano **2012**, 6, 3499– 3505 Google Scholar

18. Wang, J.; Ma, J.; Ni, Z.; Zhang, L.; Hu, G. Effects of Access Resistance on the Resistive-Pulse Caused by Translocating of a Nanoparticle Through a Nanopore RSC Adv. **2014**, 4, 7601– 7610 Google Scholar

19. Wanunu, M.; Dadosh, T.; Ray, V.; Jin, J.; McReynolds, L.; Drndic, M. Rapid Electronic Detection of Probe-Specific MicroRNAs Using Thin Nanopore Sensors Nat. Nanotechnol. **2010**, 5, 807– 814 Google Scholar

20. Heins, E. A.; Siwy, Z. S.; Baker, L. A.; Martin, C. R. Detecting Single Porphyrin Molecules in a Conically Shaped Synthetic Nanopore Nano Lett. **2005**, 5, 1824– 1829 Google Scholar

21. Vogel, R.; Willmott, G.; Kozak, D.; Roberts, G. S.; Anderson, W.; Groenewegen, L.; Glossop, B.; Barnett, A.; Turner, A.; Trau, M. Quantitative Sizing of Nano/Microparticles With a Tunable Elastomeric Pore Sensor Anal. Chem. **2011**, 83, 3499– 3506 Google Scholar

22. Willmott, G. R.; Vogel, R.; Yu, S. S. C.; Groenewegen, L. G.; Roberts, G. S.; Kozak, D.; Anderson, W.; Trau, M. Use of Tunable Nanopore Blockade Rates to Investigate Colloidal Dispersions J.Phys.: Condens. Matter **2010**, 22 Google Scholar

23. Stober, G.; Steinbock, L. J.; Keyser, U. F. Modeling of Colloidal Transport in Capillaries J. Appl. Phys. **2009**, 105 Google Scholar

24. Venta, K.; Shemer, G.; Puster, M.; Rodriguez-Manzo, J. A.; Balan, A.; Rosenstein, J. K.; Shepard, K.; Drndic, M. Differentiation of Short, Single-Stranded DNA Homopolymers in Solid-State Nanopores ACS Nano **2013**, 7, 4629– 4636 Google Scholar

25. van den Hout, M.; Krudde, V.; Janssen, X. J. A.; Dekker, N. H. Distinguishable Populations Report on the Interactions of Single DNA Molecules With Solid-State Nanopores Biophys. J. **2010**, 99, 3840– 3848 Google Scholar

26. Wanunu, M.; Sutin, J.; McNally, B.; Chow, A.; Meller, A. DNA Translocation Governed by Interactions With Solid-State Nanopores Biophys. J. **2008**, 95, 4716– 4725 Google Scholar

27. Kowalczyk, S. W.; Dekker, C. Measurement of the Docking Time of a DNA Molecule onto a Solid-State Nanopore Nano Lett. **2012**, 12, 4159– 4163 Google Scholar

28. Rosenstein, J. K.; Wanunu, M.; Merchant, C. A.; Drndic, M.; Shepard, K. L. Integrated Nanopore Sensing Platform With Sub-Microsecond Temporal Resolution Nat. Meth. **2012**, 9, 487– U112 Google Scholar

29. Vlassarev, D. M.; Golovchenko, J. A. Trapping DNA Near a Solid-State Nanopore Biophys. J. **2012**, 103, 352– 356 Google Scholar

30. Smeets, R. M. M.; Keyser, U. F.; Krapf, D.; Wu, M. Y.; Dekker, N. H.; Dekker, C. Salt Dependence of Ion Transport and DNA Translocation Through Solid-State Nanopores Nano Lett. **2006**, 6, 89– 95 Google Scholar

31. Stein, D.; Kruithof, M.; Dekker, C. Surface-Charge-Governed Ion Transport in Nanofluidic Channels Phys. Rev. Lett. **2004**, 93 Google Scholar

32. Kowalczyk, S. W.; Dekker, C. Salt and Voltage Dependence of the Conductance Blockade Induced by Translocation of DNA and RecA Filaments Through Solid-State Nanopores. In Nanopores for Bioanalytical Applications; Edel, J.; Albrecht, T., Eds.; Royal Society of Chemistry: London, 2012. Google Scholar

33. Yang, J.; Ferranti, D. C.; Stern, L. A.; Sanford, C. A.; Huang, J.; Ren, Z.; Qin, L.-C.; Hall, A. R. Rapid and Precise Scanning Helium Ion Microscope Milling of Solid-State Nanopores for Biomolecule Detection Nanotechnology **2011**, 22, 285310 Google Scholar

34. Aksimentiev, A.; Heng, J. B.; Timp, G.; Schulten, K. Microscopic Kinetics of DNA Translocation Through Synthetic Nanopores Biophys. J. **2004**, 87, 2086– 2097 Google Scholar

35. Lu, B.; Albertorio, F.; Hoogerheide, D. P.; Golovchenko, J. A. Origins and Consequences of Velocity Fluctuations During DNA Passage Through a Nanopore Biophys. J. **2011**, 101, 70– 79 Google Scholar

36. Storm, A. J.; Storm, C.; Chen, J. H.; Zandbergen, H.; Joanny, J. F.; Dekker, C. Fast DNA Translocation through a Solid-State Nanopore Nano Lett. **2005**, 5, 1193– 1197 Google Scholar

37. Chen, P.; Gu, J. J.; Brandin, E.; Kim, Y. R.; Wang, Q.; Branton, D. Probing Single DNA Molecule Transport Using Fabricated Nanopores Nano Lett. **2004**, 4, 2293– 2298 Google Scholar

38. Mandel, M. The Electrical Polarization of Rod-Like Charged Macromolecules Mol. Phys. **1961**, 4, 489– 469 Google Scholar

39. Manning, G. S. A Condensed Counterion Theory for Polarization of Polyelectrolyte Solutions in High Fields J. Chem. Phys. **1993**, 99, 477– 486 Google Scholar

40. Mohanty, U.; Zhao, Y. Q. Polarization of Counterions in Polyelectrolytes Biopolymers **1996**, 38, 377– 388 Google Scholar

41. Rau, D. C.; Charney, E. Polarization of the Ion Atmosphere of a Charged Cylinder Biophys. Chem. **1981**, 14, 1– 9 Google Scholar

42. Elvingson, C. Computer Simlations of the Structure of DNA Molecules in an Electric Field Biophys. Chem. **1992**, 43, 9– 19 Google Scholar

43. Netz, R. R. Polyelectrolytes in Electric Fields J. Phys. Chem. B **2003**, 107, 8208– 8217 Google Scholar

44. Yoshida, M.; Kikuchi, K.; Maekawa, T.; Watanabe, H. Electric Polarization of Rodlike Polyions Investigated by Monte-Carlo Simulations J. Phys. Chem. **1992**, 96, 2365– 2371 Google Scholar

45. Diekmann, S.; Hillen, W.; Jung, M.; Wells, R. D.; Porschke, D. Electric Properties and Structure of DNA Restriction Fragments From Measurements of the Electrical Dichroism Biophys. Chem. **1982**, 15, 157– 167 Google Scholar

46. Diekmann, S.; Jung, M.; Teubner, M. On the Orientation Function of the Electric Dichroism of DNA J. Chem. Phys. **1984**, 80, 1259– 1262 Google Scholar

47. Porschke, D. The Mechanism of Ion Polarization Along DNA Double Helices Biophys. Chem. **1985**, 22, 237– 247 Google Scholar

48. Chang, H.; Venkatesan, B. M.; Iqbal, S. M.; Andreadakis, G.; Kosari, F.; Vasmatzis, G.; Peroulis, D.; Bashir, R. DNA Counterion Current and Saturation Examined by a MEMS-Based Solid State Nanopore Sensor Biomed. Microdevices **2006**, 8, 263– 269 Google Scholar

49. Das, S.; Dubsky, P.; van den Berg, A.; Eijkel, J. C. T. Concentration Polarization in Translocation of DNA Through Nanopores and Nanochannels Phys. Rev. Lett. **2012**, 108 Google Scholar

50. Comer, J.; Dimitrov, V.; Zhao, Q.; Timp, G.; Aksimentiev, A. Microscopic Mechanics of Hairpin DNA Translocation Through Synthetic Nanopores Biophys. J. **2009**, 96, 593– 608 Google Scholar

51. Luan, B.; Aksimentiev, A. Electro-Osmotic Screening of the DNA Charge in a Nanopore Phys. Rev. E **2008**, 78 Google Scholar

52. Yoo, J.; Aksimentiev, A. Competitive Binding of Cations to Duplex DNA Revealed Through Molecular Dynamics Simulations J. Phys. Chem. B **2012**, 116, 12946– 12954 Google Scholar

53. Singer, A.; Rapireddy, S.; Ly, D. H.; Meller, A. Electronic Barcoding of a Viral Gene at the Single-Molecule Level Nano Lett. **2012**, 12, 1722– 1728 Google Scholar

54. Garaj, S.; Hubbard, W.; Reina, A.; Kong, J.; Branton, D.; Golovchenko, J. A. Graphene as a Subnanometre Trans-Electrode Membrane Nature **2010**, 467, 190– U73 Google Scholar

55. Garaj, S.; Liu, S.; Golovchenko, J. A.; Branton, D. Molecule-Hugging Graphene Nanopores Proc. Natl. Acad. Sci. U.S.A. **2013**, 110, 12192– 12196 Google Scholar

56. Merchant, C. A.; Healy, K.; Wanunu, M.; Ray, V.; Peterman, N.; Bartel, J.; Fischbein, M. D.; Venta, K.; Luo, Z. T.; Johnson, A. T. C.DNA Translocation Through Graphene Nanopores Nano Lett. **2010**, 10, 2915– 2921 Google Scholar

57. Schneider, G. F.; Kowalczyk, S. W.; Calado, V. E.; Pandraud, G.; Zandbergen, H. W.; Vandersypen, L. M. K.; Dekker, C. DNA Translocation Through Graphene Nanopores Nano Lett. **2010**, 10, 3163– 3167 Google Scholar

58. Traversi, F.; Raillon, C.; Benameur, S. M.; Liu, K.; Khlybov, S.; Tosun, M.; Krasnozhon, D.; Kris, A.; Radenovic, A. Detecting the Translocation of DNA Through a Nanopore Using Graphene Nanoribbons Nat. Nanotechnol. **2013**, 8, 939– 945 Google Scholar

59. Marshall, M. M.; Yang, J.; Hall, A. R. Direct and Transmission Milling of Suspended Silicon Nitride Membranes With a Focused Helium Ion Beam Scanning **2012**, 34, 101– 106 Google Scholar

60. Hall, A. R. *In Situ* Thickness Assessment During Ion Milling of a Free-Standing Membrane Using Transmission Helium Ion Microscopy Microsc. Microanal. **2013**, 19, 740– 744 Google Scholar

Supporting Information

Interpreting the Conductance Blockades of DNA Translocations Through Solid-State Nanopores

Autumn T. Carlsen, Osama K. Zahid, Jan Ruzicka, Ethan W. Taylor, and Adam R. Hall

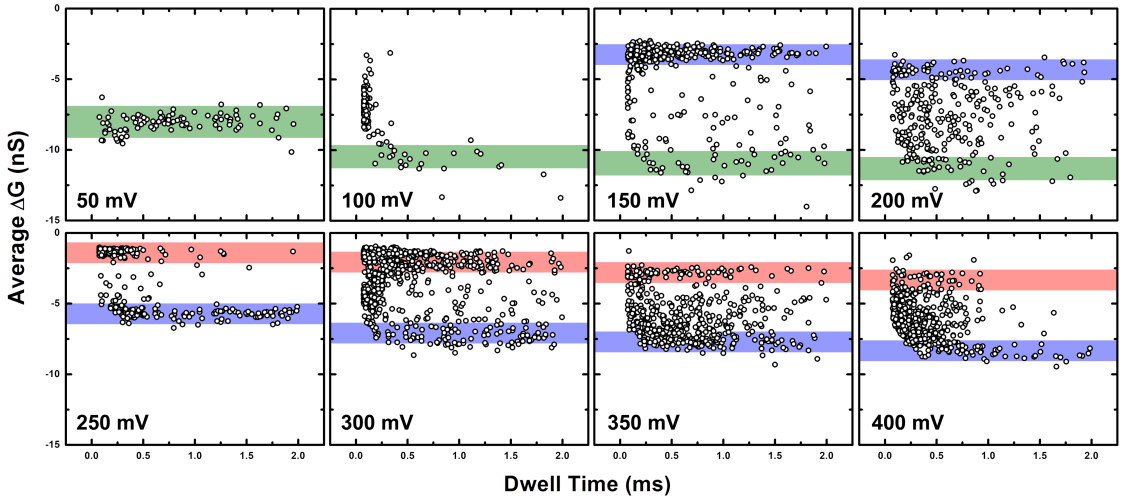

Figure S-1. Scatter plots of blockade events. Event depth (ΔG) vs. dwell time (Δt) for all recorded events at each voltage (same data as shown in Fig. 1c of the main text). Shaded regions correspond to the three interaction types described in the text, with the same color scheme as in Figs. 1 and 3. Events consisting of multiple levels reside between the shaded regions.

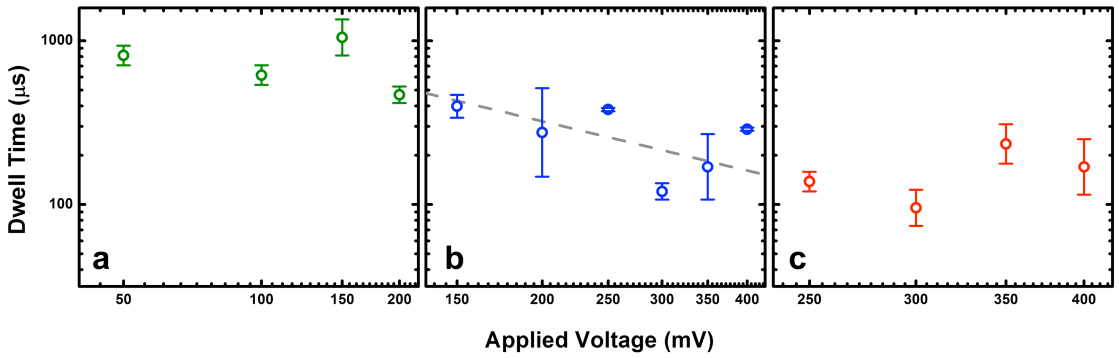

Figure S-2. Event dwell times. Voltage dependence of mean dwell time for events observed in the three types of DNA-pore interactions described in the text: lateral blocking (a), translocation (b), and interaction with one access region (c). Only single-level events are considered. For measurements ≥250 mV, we frequently observe two populations in the translocation data, one of which yields a dwell time >1 ms. We attribute these long duration events to strong interactions between the DNA and the pore and/or the surrounding membrane, and so we plot only the shorter duration populations here. Data shown in (a) and (c) exhibit no voltage dependence[1] over the range studied, indicating that forces other than electrical (e.g. diffusive[2]) dominate. Dashed line in (b) is a 1/V fit to the data, similar to that reported elsewhere[3].

S1. Employing the conductance model to analyze published experimental results The simple model presented in the main text utilizes free parameters that can be adjusted to predict the saturation conductance change, ΔG, for a wide range of experimental conditions. We have identified three previous works that report voltage dependence of ΔG for dsDNA[4-6]. In order to verify the utility of our approach, we employ our model to predict the maximum conductance change under the experimental conditions associated with each of these data sets. Note that we use the model describing full translocation events (see Fig. 2 in the main text) and assume all counterions are locally displaced (β=0, see Fig. 4 in the main text).

First, we consider the work of Kowalczyk, *et al.*[4], which describes high-ionic strength measurements in different solvents. From the materials description, we take the SS-nanopore diameter, d_p, as 21 nm and the effective membrane thickness, L_{eff}, as 6.7 nm. Recall that we use the experimentally-determined[7] convention $L_{eff}=L/3$, where L is initial membrane thickness (20 nm in this case). In Fig. S-3, we show data for 1 M KCl (a), 1 M NaCl (b), and 1 M LiCl (c) overlaid with the ΔG calculated from our model (dashed lines), taking into consideration the electrophoretic mobilities of the three different cations. We find that the model's prediction correlates very well with the ΔG measured at high voltage, where the conductance curve approaches saturation.

A second example, published by Yang, *et al.*[6], is presented in a similar way in Fig. S-3d. Here, values of d_p=24.7 nm, L_{eff}=14.2 nm, and a solvent condition of 1 M KCl are plugged into the model, which yields a ΔG prediction (dashed line) that matches the experimental results within error.

Finally, we consider the results of Skinner, *et al*.[5], for which conditions of d_p=10 nm, L_{eff}=6.7 nm, and a 1 M KCl solvent are used (Fig. S-3e). In this case, we find significant discrepancy between the prediction (dashed line) and the apparent saturation level of the ΔG. However, we note that the authors characterize the group of SS-nanopores used in these experiments as "approximately 10 nm in diameter"[5], implying that some deviation from this value may be present in the specific device used to collect the data. For comparison, we also plot the value predicted for the same experimental conditions, but with a slightly adjusted d_p of 15 nm (solid line), and find significantly better agreement.

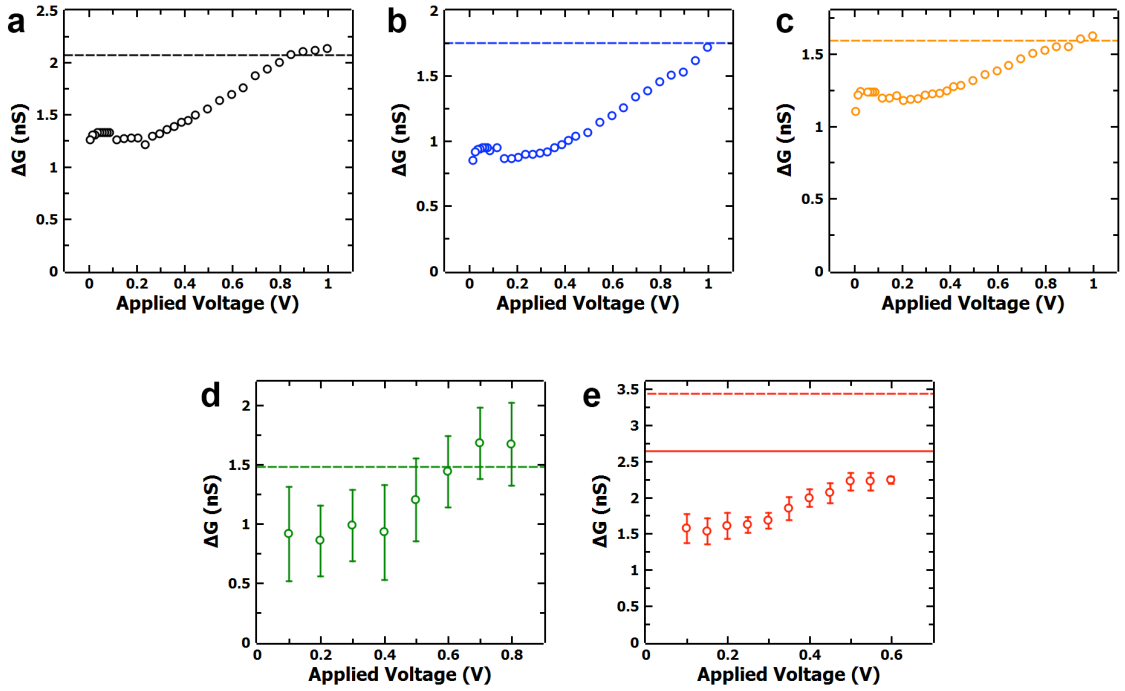

Figure S-3. Application of model to other published results Voltage-dependence of *ΔG* for dsDNA from Supplementary Reference 1 (a: 1 M KCl, b: 1 M NaCl, and c: 1 M LiCl), Supplementary Reference 2 (d), and Supplementary Reference 3 (e). Dashed lines represent the predictions of (saturated) *ΔG* from our model, considering the experimental conditions listed in the respective reports. The solid line in (e) represents the model output for a nanopore diameter of 15 nm (as described in Supplementary text S1).

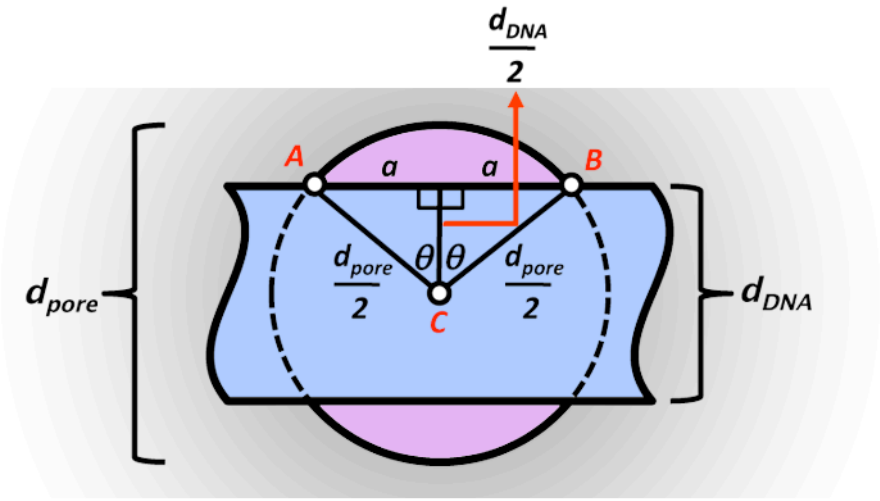

Figure S-4. Geometric model of lateral blocking of SS-nanopore Schematic of dsDNA (blue) laying laterally across a SS-nanopore (area enclosed by black circle). The areas shaded in purple represent the remaining accessible area of the blocked nanopore.

S2. Geometric expression of DNA blocking a SS-nanopore laterally The unoccluded area of the laterally-blocked SS-nanopore is composed of two segments of the circular pore, defined by the intersection of the dsDNA with the pore circumference (purple shaded regions in Fig. S-4). The area of one such segment, A_{seg}, can be expressed geometrically as

$$A_{seg} = A_{arc} - 2A_T, \qquad \text{Eq. S-1}$$

where A_{arc} is the area of the sector ABC and A_T is the area of one of the two right triangles defined by the same three points (blue regions in Fig. S-4). In terms of the known experimental quantities (nanopore diameter, d_p, and dsDNA diameter, d_{DNA}), A_{arc} can be written as

$$A_{arc} = \frac{d_p^2}{4}\theta = \frac{d_p^2}{4}\left(\cos^{-1}\left(\frac{d_{DNA}}{d_p}\right)\right). \qquad \text{Eq. S-2}$$

Line segment a at the base of the two right triangles is defined as $\frac{1}{2}(d_p^2 - d_{DNA}^2)^{\frac{1}{2}}$, and so A_T can be expressed as

$$A_T = \frac{1}{8} d_{DNA}\left(d_p^2 - d_{DNA}^2\right)^{1/2}. \qquad \text{Eq. S-3}$$

Treating the unoccluded area of the laterally blocked pore as a circular region of area A_p^* and diameter d_p^*, we can write

$$A_p^* = \frac{\pi}{4} d_p^{*2} = 2A_{seg} = \frac{d_p^2}{2}\cos^{-1}\left(\frac{d_{DNA}}{d_p}\right) - \frac{1}{2} d_{DNA}\left(d_p^2 - d_{DNA}^2\right)^{1/2}, \qquad \text{Eq. S-4}$$

and therefore

$$d_p^* = \sqrt{\frac{2}{\pi}\left(d_p^2 \cos^{-1}\left(\frac{d_{DNA}}{d_p}\right) - d_{DNA}\left(d_p^2 - d_{DNA}^2\right)^{1/2}\right)}. \qquad \text{Eq. S-5}$$

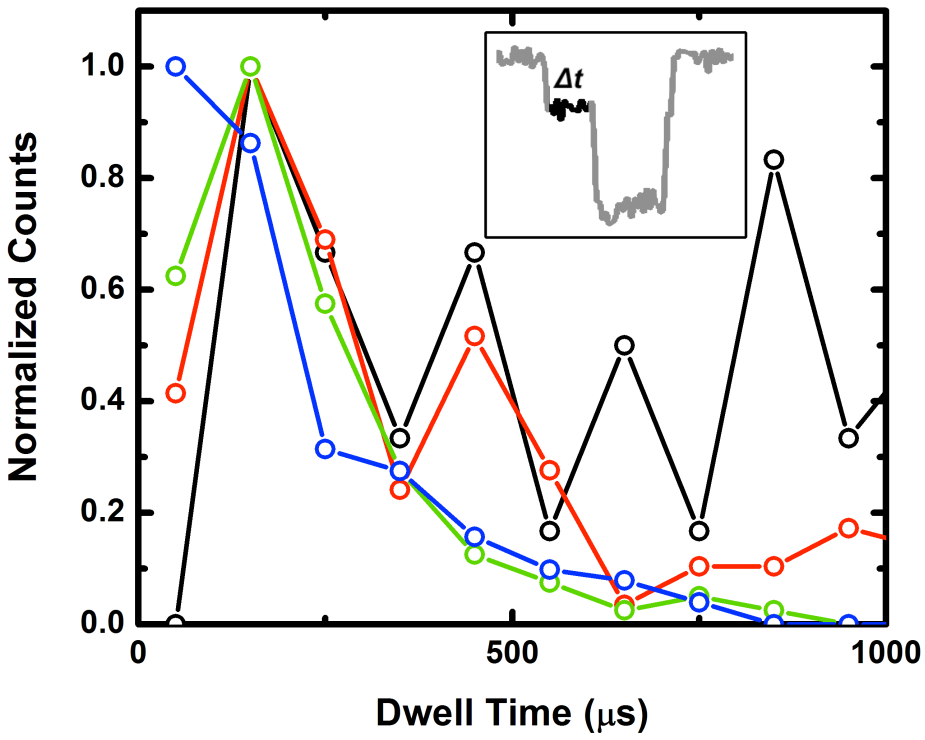

Figure S-5. Shallow-level dwell time distribution for two-level events Normalized dwell time distributions for the first (non-translocative) level in two-level events measured at 250 (black), 300 (red), 350 (green) and 400 mV (blue), respectively. As applied voltage rises, the dwell time distribution narrows and the mean dwell time is reduced. Inset highlights the section considered (black region in trace).

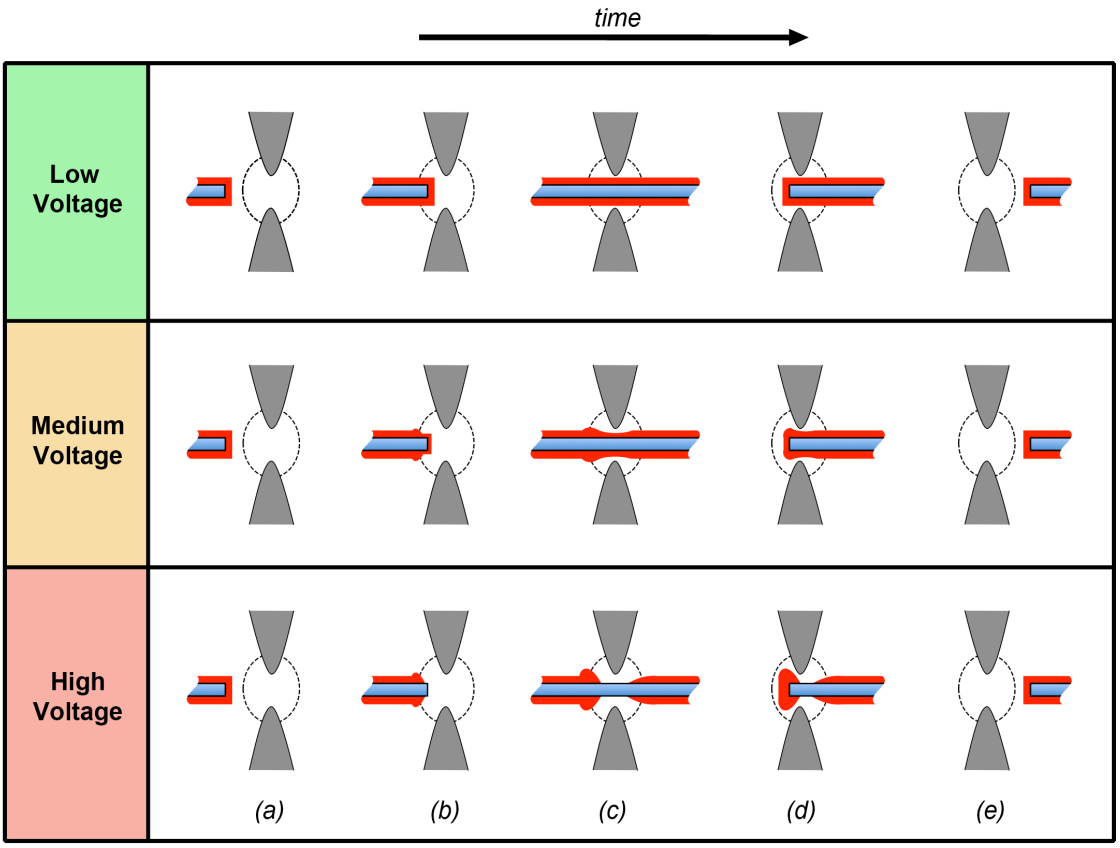

Figure S-6. Proposed mechanism of local counterion depletion by field polarization Schematic representation of proposed counterion configuration (red) surrounding DNA (blue) during translocation at low, medium, and high voltage (i.e. electric field). DNA is shown sequentially before entry (a), during entry (b), fully threaded (c), exiting (d) and fully ejected (e). As field strength increases, polarization causes depletion of counterions *local to the sensing region* (dashed lines); the buildup of charge outside this region preserves electroneutrality in the system as a whole. We note that this model suggests a significant increase in counterion density at the trailing end of the DNA (d), but this effect would be difficult to resolve experimentally due to temporal limitations[8].

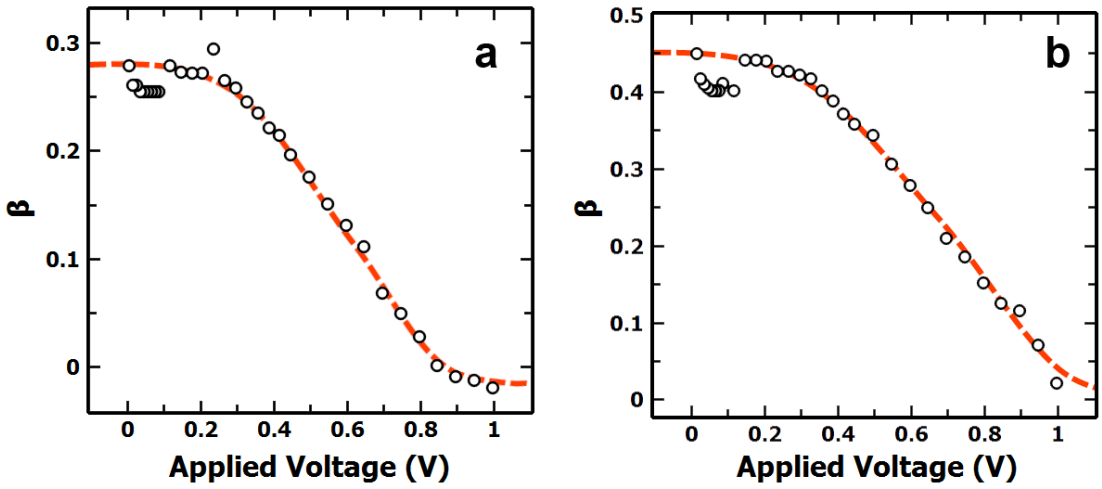

Figure S-7. Estimation of local counterion density on dsDNA at zero field Fractional counterion density β vs. applied voltage for both the 1 M KCl data (a) and the 1 M NaCl data (b) from Supplementary Reference 1. β is adjusted in our model to account for the shifting ΔG in the data, yielding a sigmoidal relation. The low-voltage limit appears to fall at about 0.28 for 1 M KCl and about 0.45 for 1 M NaCl. The latter is near the NaCl data from the main text (Fig. 4), which yields a limit of roughly 0.57. The deviation may result from lower ionic strength used in our experiments (900 mM) compared to these data. Dashed lines are Boltzmann sigmoidal fits.

S3. Analysis of conductance blockade levels for small-diameter SS-nanopores Recent work by Wanunu, *et al*.[2] and van den Hout, *et al*.[9] explored the conductance signal resulting from measurements on dsDNA with SS-nanopores of diameter ~2-5 nm. Both reported the unexpected observation of multiple, discrete populations of ΔG and speculated that they originated from spurious (non-translocative) interactions with the pore.

Because our model can account for multiple ΔG levels (translocative and single-access-region interactions), we used it to analyze the results from both groups. In Fig. S-8, we plot all data from the two papers (Fig. 6 from Supplementary Reference 7 and Fig. S4 from Supplementary Reference 8) using the convention from those reports that defines I_B as the relative current blockade ($I_B = I_{blocked}/I_0$, where $I_{blocked}$ is the ionic current during the blockade and I_0 is the open pore ionic current). All data were taken on comparable devices and follow the same trends. In their initial reports, both groups used basic geometric models to attribute the low-level current blockade (green population in Fig. S-8) to pore occlusion. However, the high-level population (red) was not easily rationalized. Using the experimental conditions given in the two reports, we find (Fig. S-8) that our models for translocation (solid line) and access region interactions (dashed line) capture the trends of both populations qualitatively and achieve good quantitative agreement if we assume a β of 0.11. Considering that a voltage of 300 mV was applied in these measurements and that the saturating blockade level usually does not occur until considerably higher applied voltages (c.f. Fig. S-3), this value of β is reasonable. We predict that measurements taken at higher voltage would yield similar results to those

reported by the two groups, but both populations would be shifted to lower I_B (that is, larger ΔG).

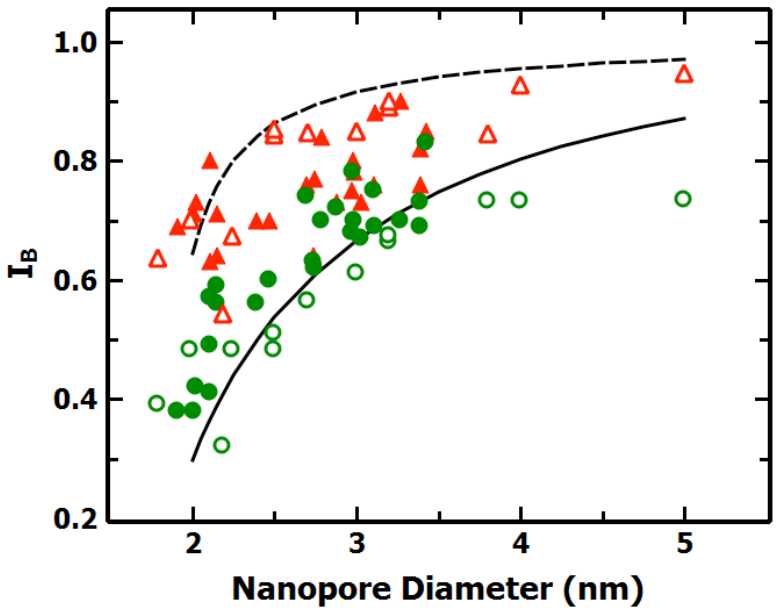

Figure S-8. Interpretation of published small-diameter SS-nanopore data Plotted data points are from Supplementary Reference 5 (solid symbols) and Supplementary Reference 6 (hollow symbols) recorded at 300 mV. Green circles represent the low-current level population and red triangles represent the high-current level population. The dashed and solid lines are predictions from our presented model (solid line represents the translocative model; dashed line represents the access region level) using the experimental parameters given in the respective references and assuming β=0.11.

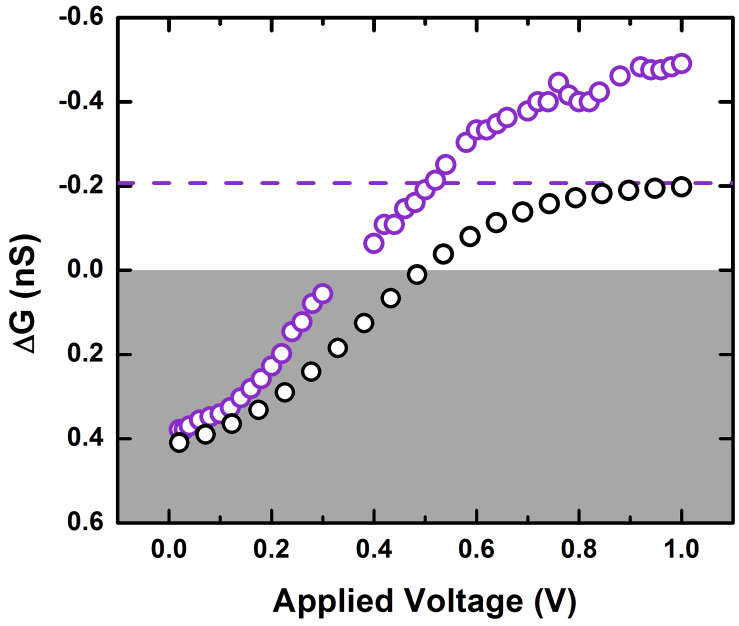

Figure S-9. Application of model interpretation to measurements in low ionic strength solvent Purple circles are data for 0.1 M KCl from Supplementary Reference 1. The shaded region represents conductance *increases*. The dashed line is the value predicted from our model for β=0. Black circles represent expectations from the model with β ranging from 0.22 to 0. Adjusting β with applied voltage based on a Boltzmann sigmoidal fit to the experimental data, we demonstrate that, in spite of quantitative disagreement with the experimental saturation level (~0.5 nS), the model captures a major qualitative feature of the low-ionic strength data: a switch from conductance blockades to enhancements as voltage is reduced.

Supplementary References

1. Kasianowicz, J. J.; Brandin, E.; Branton, D.; Deamer, D. W. Characterization of Individual Polynucleotide Molecules Using a Membrane Channel. *Proc. Natl. Acad. Sci. U. S. A.* 1996, 93, 13770-13773.

2. Wanunu, M.; Sutin, J.; McNally, B.; Chow, A.; Meller, A. DNA Translocation Governed By Interactions with Solid-State Nanopores. *Biophys. J.* 2008, 95, 4716-4725.

3. Kowalczyk, S. W.; Dekker, C. Measurement of the Docking Time of a DNA Molecule Onto a Solid-State Nanopore. *Nano Lett.* 2012, 12, 4159-4163.

4. Kowalczyk, S. W.; Dekker, C. Salt and Voltage Dependence of the Conductance Blockade Induced By Translocation of DNA and RecA Filaments Through Solid-State Nanopores. In *Nanopores for Bioanalytical Applications*, Edel, J.; Albrecht, T., Eds. Royal Society of Chemistry: 2012.

5. Skinner, G. M.; van den Hout, M.; Broekmans, O.; Dekker, C.; Dekker, N. H. Distinguishing Single- and Double-Stranded Nucleic Acid Molecules Using Solid-State Nanopores. *Nano Lett.* 2009, 9, 2953-2960.

6. Yang, J.; Ferranti, D. C.; Stern, L. A.; Sanford, C. A.; Huang, J.; Ren, Z.; Qin, L.-C.; Hall, A. R. Rapid and Precise Scanning Helium Ion Microscope Milling of Solid-State Nanopores For Biomolecule Detection. *Nanotechnol.* 2011, 22, 285310.

7. Wanunu, M.; Dadosh, T.; Ray, V.; Jin, J.; McReynolds, L.; Drndic, M. Rapid Electronic Detection of Probe-Specific MicroRNAs Using Thin Nanopore Sensors. *Nat. Nanotechnol.* 2010, 5, 807-814.

8. Das, S.; Dubsky, P.; van den Berg, A.; Eijkel, J. C. T. Concentration Polarization in Translocation of DNA Through Nanopores and Nanochannels. *Phys. Rev. Lett.* 2012, 108, 138101.

9. van den Hout, M.; Krudde, V.; Janssen, X. J. A.; Dekker, N. H. Distinguishable Populations Report On the Interactions of Single DNA Molecules With Solid-State Nanopores. *Biophysical Journal* 2010, 99, 3840-3848.